ACS OMEGA

http://pubs.acs.org/journal/acsodf

Article

Fractal-Like Kinetics of Adsorption Applied to the Solid/Solution Interface

Naoual El Bardiji, Khadija Ziat,* Ahmed Naji, and Mohamed Saidi

Cite This: *ACS Omega* 2020, 5, 5105−5115

Read Online

ACCESS | Metrics & More | Article Recommendations | Supporting Information

ABSTRACT: In this paper, the fractal-like multiexponential (f-mexp) equation was modified by introducing the fractional fractal exponent to each stage of the adsorption process. The new equation was used for the analysis of kinetic adsorption of copper onto treated attapulgite. The modeling results show that the modified f-mexp equation fits properly the kinetic data in comparison with the classical and fractal-like kinetic models tested. The effect of varying the initial concentration of the adsorbate on the kinetic parameters was analyzed. Artificial neural networks were applied for the prediction of adsorption efficiency. Outcomes indicate that the multilayer perceptron neural network can predict the removal of copper from aqueous solutions more accurately under different experimental conditions than the single-layer feedforward neural network. Single-site and multisite occupancy adsorption models were used for the analysis of experimental adsorption equilibrium data of copper onto treated attapulgite. The modeling results show that there is no multisite occupancy effect and that the equilibrium data fit well the Langmuir−Freundlich isotherm.

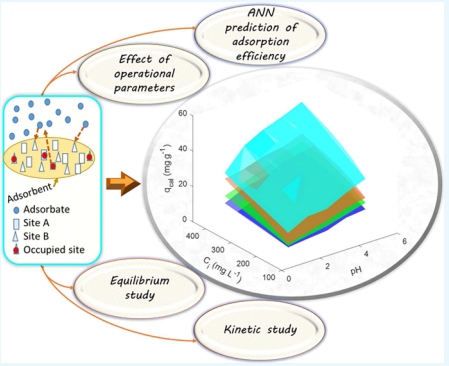

1. INTRODUCTION

The treatment of industrial wastewater is one of the essential aspects of the preservation of water resources. The conventional treatment methods include ion exchange, membrane separation, adsorption, and electrochemical process. Among them, adsorption has been one of the most successfully applied methods owing to its easy operational process and high efficiency.[1]

The precise description of the adsorption process at a solid/solution interface requires adequate mathematical expressions, for both kinetics and adsorption equilibrium, in order to determine properly the interaction mechanism occurring at a sorbent/sorbate system.[2]

The artificial neural network (ANN) is an attractive tool for predicting the sorption phenomenon.[3−6] Such a technique allows learning linear and nonlinear relationships between variables directly from a set of examples based on no assumptions concerning the nature of the phenomenological mechanisms.[3]

The adsorption isotherms are equilibrium equations that describe how adsorbates interact with the sorbent materials, thus providing some insights into the sorption mechanism, the surface properties, and the affinity of the sorbent.[7] The Langmuir[8] and Freundlich[9] isotherms are usually used to analyze adsorption equilibrium data. These models are based on the assumption that each molecule of adsorbate occupies one adsorption site of the surface with no lateral interaction. In 1984, Nitta et al.[10] derived an adsorption isotherm equation from a localized monolayer model in which lateral interactions are taken into consideration and each adsorbate molecule may occupy more than one site on a homogeneous surface. Afterward, the equation was extended to a heterogeneous surface of multisite occupancy.[11] Later on, Ramirez-Pastor et al.[12−15] developed a statistical thermodynamics model to study the adsorption of linear adsorbates for multisite occupancy on homogeneous surfaces. Recently, Riccardo et al.[16] presented a new theoretical description of the fractional statistical theory of adsorption phenomena based on Haldane's statistics for complex adsorption systems. More recently, a new distribution for systems of particles in equilibrium obeying the exclusion of correlated states was introduced following Haldane's state counting.[17]

Knowledge of kinetic features in a solid/solution system provides an insight into the possible mechanism of adsorption along with the reaction pathways.[18] Several kinetic models have been used to predict the adsorption kinetics in solid/solution interfaces. These models assume that the kinetic constants are time-invariant. This concept has been unsatisfactory, especially, when the reactants were spatially constrained by walls or phase boundaries.[19] Based on theoretical and phenomenological observations, Kopelman demonstrated

Received: December 1, 2019
Accepted: February 20, 2020
Published: March 6, 2020

https://dx.doi.org/10.1021/acsomega.9b04088
ACS Omega 2020, 5, 5105−5115

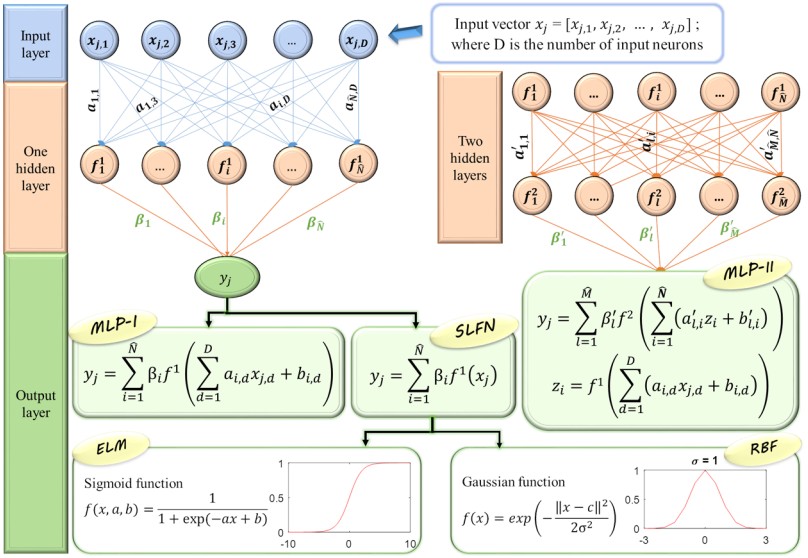

Figure 1. Architecture of SLFN and MLP with one and two hidden layers.

that the reaction rate coefficient is time-dependent (fractal-like kinetics).[19]

Recently, the fractal-like concept has been introduced and used to analyze adsorption kinetics for both homogeneous and heterogeneous systems.[20−23] In this context, we have proposed some modifications to the fractal-like multiexponential equation and derived a new equation for kinetics of adsorption called modified fractal-like multiexponential (modified f-mexp). The applicability of the new equation was verified for different concentrations of copper adsorption onto treated attapulgite (TATP). Afterward, the modeling results were compared to those of classical and fractal-like kinetic equations. Included in this paper is also the investigation of the effect of parameters such as pH of the solution, initial concentration of the solute, and the dose of adsorbent on the efficiency of copper adsorption on TATP, along with the modeling analysis of equilibrium data by models for a single-site and multisite occupancy adsorption and by ANNs.

2. THEORETICAL ANALYSIS

2.1. ANN Models. ANNs are computer systems based on the functioning mechanism of the brain. The architecture of ANN is composed of an input layer with input parameters, one or plus hidden layers, and an output layer. The input parameters are linearly combined into a hidden layer of units where new combinations are created as final output variables. Knowledge of the number of network layers, the number of neurons in the layers, and the learning algorithms and the neuron transfer functions is essential for the effective design of the architecture of ANN.[24] An exhaustive bibliography for neural network models can be found in refs 25−33.

Figure 1 shows the structure of the extreme learning machine (ELM) and the radial basis function (RBF) for the single-layer feedforward neural network (SLFN) and multilayer perceptron (MLP) with one or two hidden layers. It comprises an input layer with N input vectors, one or two hidden layers with $\hat{N}$ or $\hat{M}$ neurons, and an output layer with one neuron.

In this work, ANN's architecture is composed of an input layer with 3 neurons (pH, adsorbent dose, and initial solute concentration), a hidden layer with 10 neurons and an output layer with 1 neuron (adsorbed amount at equilibrium). ELM, RBF, and MLP neural network models were used to predict the responses corresponding to 120 experimental points. A three- and four-layer perceptron was investigated by using MATLAB version R2015a software. The ELM model was analyzed by the same version of MATLAB software, while the RBF model was tested by using IBM-SPSS version 20 software. For ELM and RBF models, the data were randomly segregated into a training data set (75%) and testing data set (25%). For MLP, data were divided into 50% for the training data set, 25% for validating data set, and 25% for testing data set. In addition to that, the Levenberg−Marquardt (LM) and Bayesian regularization backpropagation (BRB) training algorithms were tested. The MATLAB code of ELM and MLP models is shown in Supporting Information.

2.2. Adsorption Models. *2.2.1. Adsorption equilibrium isotherms.* A century ago, Langmuir[8] presented an isotherm equation to study the adsorption for gas-phase processes

$$q = \frac{K_e q_{max} p}{1 + K_e p} \tag{1}$$

or

$$K_e = \frac{\theta}{p(1-\theta)} \tag{2}$$

where K_e (Pa^{-1}) is the equilibrium constant, q_{max} (mg g^{-1}) is the theoretical monolayer capacity, p (Pa) is the equilibrium pressure, and $\theta = q/q_{max}$ is the coverage.

The Langmuir isotherm for gas-phase processes was used for the analysis of adsorption from solutions by replacing the pressure term with the solute concentration C. We obtain the following equation

$$q = \frac{K_e q_{max} C}{1 + K_e C} \tag{3}$$

or

$$K_e = \frac{\theta}{C(1-\theta)} \tag{4}$$

where C (mg L^{-1}) is the equilibrium solute concentration.

https://dx.doi.org/10.1021/acsomega.9b04088
ACS Omega 2020, 5, 5105−5115

Table 1. Classical and Fractal-Like Adsorption Kinetic Models and Their Expressions[a]

kinetic model	rate equation	integrated equation	parameters
PFO[37]	$dq_t/dt = k_1(q - q_t)$	$q_t = q(1 - \exp(-k_1 t))$	q, k_1
f-PFO[21]	$dq_t/dt = k_1' t^{-h}(q - q_t)$	$q_t = q\left[1 - \exp\left(\frac{-k_1'}{1-h} t^{(1-h)}\right)\right]$	q, k_1', h
PSO[38]	$dq_t/dt = k_2(q - q_t)^2$	$q_t = \frac{k_2 q^2 t}{1 + k_2 q t}$	q, k_2
f-PSO[21]	$dq_t/dt = k_2' t^{-h}(q - q_t)^2$	$q_t = \frac{\frac{k_2'}{1-h} q^2 t^{(1-h)}}{1 + \frac{k_2'}{1-h} q t^{(1-h)}}$	q, k_2', h
MO[40]	$\frac{dF}{dt} = \frac{k_1}{1 - f_2}(1 - F)(1 - f_2 F)$	$q_t = q\frac{1 - \exp(-k_1 t)}{1 - f_2 \exp(-k_1 t)}$	q, k_1, f_2
f-MO[21]	$\frac{dF}{dt} = \frac{k_1' t^{-h}}{1 - f_2}[(1 - F)(1 - f_2 F)]$	$q_t = q\frac{1 - \exp\left(\frac{-k_1'}{1-h} t^{(1-h)}\right)}{1 - f_2 \exp\left(\frac{k_1'}{1-h} t^{(1-h)}\right)}$	q, k_1', f_2, h
mexp[39]	$dF/dt = \sum_{i=1}^{n} f_i k_i (1 - F_i)$	$q_t = q\left[1 - \sum_{i=1}^{n} f_i \exp(-k_i t)\right]$	q, k_i, f_i
f-mexp[23]	$dF/dt = \sum_{i=1}^{n} f_i k_i' t^{-h}(1 - F_i)$	$q_t = q\left[1 - \sum_{i=1}^{n} f_i \exp\left(-\frac{k_i'}{1-h} t^{(1-h)}\right)\right]$	q, k_i', f_i, h

[a] k_1 (min^{-1}) and k_2 (g mg^{-1} min^{-1}) are the PFO and PSO kinetic constants. k_1' ($min^{-(1-h)}$) and k_2' (g mg^{-1} $min^{-(1-h)}$) are the kinetic constants of the fractal-like PFO and PSO models. $F = q_t/q$ is the adsorption progress and $f_2 = \frac{k_2 q}{k_1 + k_2 q}$ is the parameter determining the "share" of the second-order term, n is the number of exponential terms, and k_i and k_i' are the kinetic constants of the i-th process for the mexp and f-mexp equations. f_i (i = 1, 2, ..., n), where $\sum_{i=1}^{n} f_i = 1$, are the parameters of the mexp and f-mexp models.

The Freundlich isotherm equation for adsorption from solutions is given by the expression[34]

$$q = K_F C^{1/s} \tag{5}$$

where K_F is the Freundlich constant and s is the heterogeneity constant.

Langmuir–Freundlich isotherm which is a derivative of Langmuir isotherm for energetically heterogeneous solids was successfully applied for the analysis of adsorption from solutions.[23,35,36] It is given by the following equation

$$q = \frac{K_{LF} C^{1/s}}{1 + a_{LF} C^{1/s}} \tag{6}$$

where K_{LF} and a_{LF} are the Langmuir–Freundlich constants.

The three models assume that each adsorbate species occupies one adsorption site of the surface with no lateral interaction.

Nita et al.[10] modified eq 2 by including multisite-occupancy adsorption. The multisite Langmuir (MSL) isotherm is proposed as follows

$$K_e = \frac{1}{p}\frac{\theta}{(1 - \theta)^k} \tag{7}$$

where k is the number of sites.

Later on, Ramirez-Pastor et al.[12−15] presented a model of linear adsorbates (MLA) on homogeneous surfaces, which is based on exact forms for the thermodynamic functions of linear adsorbates in one dimension and its generalization to higher dimensions. The resulting equation is proposed as follows

$$K_e = \frac{1}{p}\frac{\theta\left[1 - \frac{(k-1)}{k}\theta\right]^{k-1}}{(1 - \theta)^k} \tag{8}$$

In the limiting case k = 1, the MLA and MSL models reduce to the Langmuir isotherm (eq 2).

Equations 7 and 8 can be used to analyze adsorption from solutions by replacing the pressure term with the solute concentration. One obtains the equations in the following forms

$$K_e = \frac{1}{C}\frac{\theta}{(1 - \theta)^k} \tag{9}$$

$$K_e = \frac{1}{C}\frac{\theta\left[1 - \frac{(k-1)}{k}\theta\right]^{k-1}}{(1 - \theta)^k} \tag{10}$$

2.2.2. Classical and Fractal-Like Kinetic Models. The theoretical backgrounds of classical kinetic models of pseudo-first-order (PFO), pseudo-second-order (PSO), mixed-1,2 order (MO), and multiexponential (mexp) can be found in refs 37−40.

The fractal-like approach allows the description of the adsorption behaviors at the solid/solution interface occurring in fractal spaces. The rate coefficient with temporal "memories" is presented as[19]

$$k_f = k' t^{-h} \qquad 0 \le h \le 1,\ t \ge 1 \tag{11}$$

where k_f is the instantaneous rate coefficient, k' is the time-independent rate coefficient, and h is the fractal exponent, measuring the dimensionality of the fractal system.[41]

In 2012, Haerifar and Azizian introduced the time dependency of the adsorption rate coefficient to the PFO,

https://dx.doi.org/10.1021/acsomega.9b04088
ACS Omega 2020, 5, 5105−5115

PSO, and mixed-1,2 order equations.[21] Recently, we have introduced this concept to the multiexponential equation.[23]

Table 1 lists the classical and fractal-like kinetic equations.

The fractal-like multiexponential kinetic equation can be considered as a series of parallel fractal-like first-order equations, where each kinetic process "i" is characterized by its fractal instantaneous rate coefficient k_{f_i}

$$k_{f_i} = k_i' t^{-h} \qquad 0 \le h \le 1, \ t \ge 1 \tag{12}$$

In this case, the fractal exponent h is the same for all processes. It should be emphasized, however, that each process is governed by its adsorption stage (fast, slow...).[39] In order to take into consideration the fractal behavior in various stages of the adsorption, we introduced the fractional fractal exponent to each stage of the process. Based on the Kopelman fractal-like kinetics concept[19] applied to each process "i", the instantaneous rate coefficient can be written as

$$k_{f_i} = k_i' t^{-h_i} \qquad 0 \le h_i \le 1, \ t \ge 1 \tag{13}$$

where h_i is the fractional fractal exponent of i-th process.

By inserting eq 13 into the multiexponential rate equation (see Table 1), one obtains the modified fractal-like multiexponential rate equation

$$\frac{dF}{dt} = \sum_{i=1}^{n} f_i \frac{dF_i}{dt} = \sum_{i=1}^{n} f_i k_i' t^{-h_i} (1 - F_i) \tag{14}$$

The integrated form of eq 14 is

$$F = 1 - \sum_{i=1}^{n} f_i \exp\left(-\frac{k_i'}{1 - h_i} t^{(1-h_i)}\right) \tag{15}$$

or

$$q_t = q\left[1 - \sum_{i=1}^{n} f_i \exp\left(-\frac{k_i'}{1 - h_i} t^{(1-h_i)}\right)\right] \tag{16}$$

when $h_i = 0$, the rate equation of the modified f-mexp reduces to the classical model. The MATLAB code of the modified f-mexp is shown in Supporting Information.

2.3. Model Performance Indicators. The parameters of equilibrium, kinetic, and neural network studies were estimated using a nonlinear regression method provided by MATLAB R2017b software. The comparison between the performances of the models was evaluated based on the statistical parameters such as the chi-squared error (χ^2) and the determination coefficient (R^2). Their mathematical expressions are[23,42]

$$\chi^2 = \sum_{j=1}^{N} \frac{(q_{\mathrm{exp},j} - q_{\mathrm{cal},j})^2}{q_{\mathrm{cal},j}} \tag{17}$$

$$R^2 = \frac{\sum_{j=1}^{N} (q_{\mathrm{exp},j} - \overline{q}_{\mathrm{cal}})^2}{\sum_{j=1}^{N} (q_{\mathrm{exp},j} - \overline{q}_{\mathrm{cal}})^2 + \sum_{j=1}^{N} (q_{\mathrm{exp},j} - q_{\mathrm{cal},j})^2} \tag{18}$$

where q_{exp} and q_{cal} (mg g^{-1}) are the experimental and calculated adsorbed amount, respectively, whereas $\overline{q}_{\mathrm{cal}}$ (mg g^{-1}) refers to the average of the calculated adsorbed amount.

3. RESULTS AND DISCUSSION

Figure 2 shows the quantity of the surface charge of ATP and TATP versus pH for three ionic strengths. The three curves are identical and intersect at the same point. This result confirms that the surface charge is independent of ionic strength. The increase in pH leads to the increment in the negative charge of the quantity of the surface charge. From the curves, the average value of the point of zero charge (PZC) is 9.15 for ATP, while it is 4 for TATP. The high value of PZC of ATP is ascribed to the presence of carbonate groups such as calcite and dolomite (see the X-ray diffractograms of ATP and TATP presented in Figure S1 in Supporting Information). Indeed, the PZC values of calcite vary from 8 to 10.8.[43] The acid treatment of ATP causes a shift in the PZC from 9.15 to 4. This high shift is mainly due to the elimination of calcite and dolomite. Similar findings were reported by Frini-Srasra and Srasra.[44]

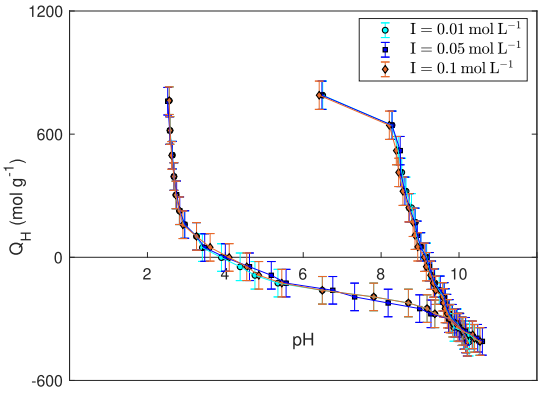

Figure 2. Variation of Q_H with pH at different ionic strengths for ATP (right) and TATP (left).

Table 2 lists the fitting values of error functions for single-layer feedforward (ELM and RBF) and MLP (MLP-LM and MLP-BRB) neural networks models. The effect of the number of hidden layers on the predictive performance was examined, and the results are also presented in Table 2. Outcomes indicate that the increase in the number of hidden layers leads to a slight improvement in the fitting results. Also from Table 2, it can be seen that the MLP models can predict the removal efficiency of copper from aqueous solutions more accurately than the SLFN models. Moreover, the MLP model with BRB resulted in a slightly better performance. It should be emphasized, however, that the MLP-LM model requires only 20 iterations, while the MLP-BRB requires 1000 iterations, which may suggest that the MLP-LM model is more effective in terms of reducing the response time.

Table 2. Results of the Neural Network Models for Predicting the Adsorbed Amount of TATP-Cu

ANN type	model	number of hidden layers	activation function	R^2	χ^2
SLFN	ELM	1	Sigmoid	0.961	28.618
	RBF	1	Gaussian	0.944	34.842
MLP	MLP-LM	1	Sigmoid	0.994	4.687
	MLP-LM	2		0.997	1.893
	MLP-BRB	1		0.998	1.214
	MLP-BRB	2		0.999	0.610

Figure 3 illustrates the predicted values of the adsorbed amount as a function of initial copper concentration at different pHs and adsorbent doses based on the MLP-BRB neural network model. Outcomes indicate that the amount of adsorption per unit mass of the adsorbent increases by increasing the solution pH or the initial concentration of

https://dx.doi.org/10.1021/acsomega.9b04088
ACS Omega 2020, 5, 5105−5115

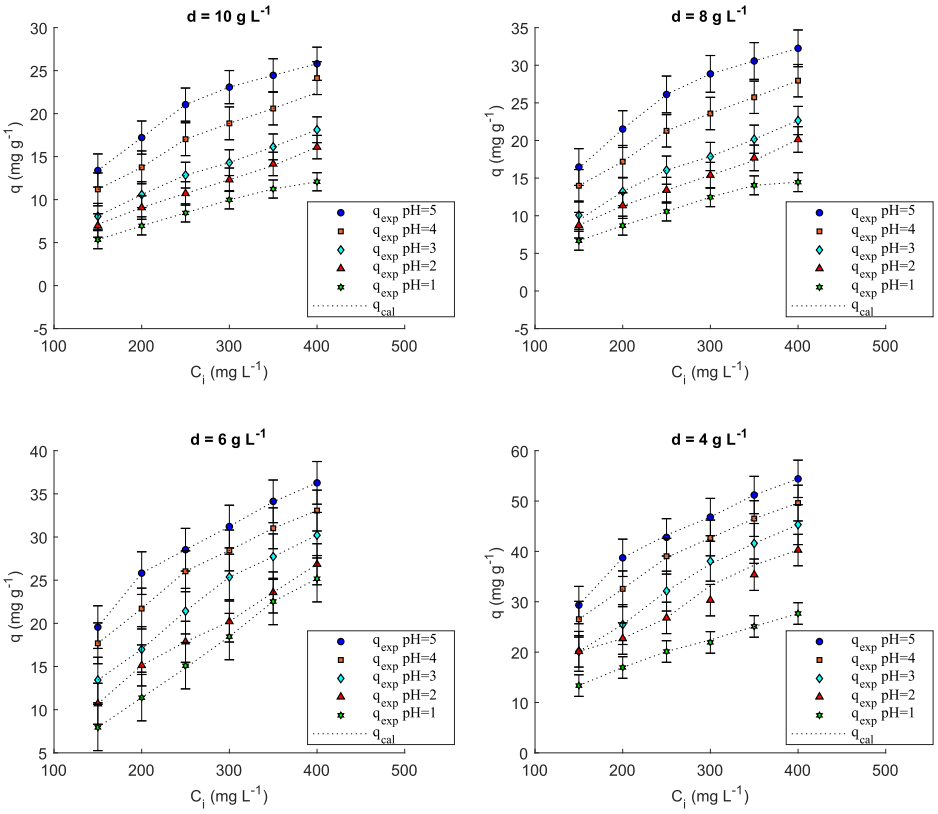

Figure 3. Adsorption profiles of copper onto TATP at various pHs, initial concentrations of solute, and adsorbent doses. Comparison between experimental data (symbols) and by fitting with the MLP-BRB (dashed lines) neural network model.

Table 3. Nonlinear Isotherm Parameters Obtained for Equilibrium Adsorption of Copper onto TATP (C_i = 150−450 mg L^{-1}, pH = 4.5, and d = 8 g L^{-1})

isotherm	Langmuir	Freundlich	Langmuir−Freundlich	MSL	MLA
parameters	q_{max} = 33.047	s = 3.864	s = 2.243	k = 1	k = 1
	K_e = 0.084	K_F = 8.298	K_{LF} = 6.772	K_e = 0.084	K_e = 0.084
			a_{LF} = 0.118		
R^2	0.867	0.994	0.998	0.867	0.867
χ^2	0.696	0.034	0.014	0.696	0.696

solute. At lower pH values, the adsorption of copper may be hindered by two effects: (1) the hydrogen ion concentration was high and the positively charged hydrogen might compete for the binding sites on the surfaces of TATP. (2) Copper ions can form complexes with the excess of chloride ions produced by the addition of HCl when adjusting the solution pH.[45,46] The increase in the pH value leads to the increment in the adsorption of metal ions. In fact, the copper adsorption depends upon the mixed effect of sorbing species and the surface properties of TATP. Taking into consideration the PZC value of TATP (PZC = 4), at pH value lower than this value, the surface of TATP is positively charged leading to electrostatic repulsion between the sorbent and the metal cations. Thus, the adsorption could possibly take place through nonelectrostatic interaction.[46] For pH > PZC, the TATP surface is negatively charged resulting in the rise in the degree of adsorption preferably occurring by electrostatic interaction.[46]

On the other hand, the mass transfer driving force increases as the initial concentration of the solute increases, and accordingly, the adsorption rate of copper on TATP becomes faster.[47]

The rise in the adsorbent dose leads to a decrease in adsorption efficiency. This is mainly due to the unsaturation of adsorption sites and the aggregation of TATP particles, which would cause a decrease in the total surface area and an increment in the diffusional path.[48]

Equations 4−6, 9 and 10 were used for modeling the adsorption equilibrium of TATP-Cu. Table 3 lists the obtained fitting results. Outcomes indicate that there is no multisite occupancy effect (k = 1). This could be ascribed to the small size of the adsorbate in comparison with those of polyatomic adsorbates used in various studies from the literature.[10,49] The theoretical models MSL and MLA have provided the same fitting results and are identical to those of the Langmuir model. On the other hand, the equilibrium adsorption data are well interpreted by the Langmuir−Freundlich isotherm, thus suggesting an energetically heterogeneous surface for the TATP; therefore, the fractal-like kinetic models could be used to analyze kinetic data of adsorption of copper onto TATP.[22]

PFO, PSO, mixed-1,2 order, and multiexponential equations and their fractal counterparts have been used to describe the kinetic adsorption of TATP-Cu at different initial concentrations of the adsorbate. The values of the calculated

https://dx.doi.org/10.1021/acsomega.9b04088
ACS Omega 2020, 5, 5105−5115

Table 4. Fitted Parameters of mexp, f-mexp, and Modified f-mexp Models at Different Initial Concentrations of the Solute for Copper Adsorption onto TATP

	mexp			f-mexp			modified f-mexp		
C_i	parameters	i		parameters	i		parameters	i	
		1	2		1	2		1	2
150	q	15.645		q	17.468		q	17.654	
	k_i	0.8537	0.0174	k_i'	0.1332	0.1333	k_i'	0.732	0.048
	f_i	0.432	0.568	f_i	0.499	0.501	f_i	0.399	0.601
	$t_{1/2}$	5.785		h	0.679		h_i	0.963	0.405
	$t_{1/2,i}$	0.812	39.846	$t_{1/2}$	5.184		$t_{1/2}$	5.169	
				$t_{1/2,i}$	5.299	5.432	$t_{1/2,i}$	0.415	39.883
	R^2	0.975		R^2	0.961		R^2	0.995	
	χ^2	0.411		χ^2	0.569		χ^2	0.243	
200	q	19.628		q	21.899		q	21.654	
	k_i	0.9242	0.0186	k_i'	0.1375	0.1340	k_i'	0.763	0.077
	f_i	0.460	0.540	f_i	0.486	0.514	f_i	0.346	0.654
	$t_{1/2}$	4.538		h	0.695		h_i	0.963	0.405
	$t_{1/2,i}$	0.750	37.266	$t_{1/2}$	4.269		$t_{1/2}$	4.134	
				$t_{1/2,i}$	4.143	4.635	$t_{1/2,i}$	0.263	22.651
	R^2	0.987		R^2	0.985		R^2	0.996	
	χ^2	0.298		χ^2	0.312		χ^2	0.164	
250	q	22.645		q	24.399		q	24.365	
	k_i	0.9258	0.0258	k_i'	0.1444	0.1502	k_i'	0.781	0.101
	f_i	0.435	0.565	f_i	0.495	0.505	f_i	0.233	0.767
	$t_{1/2}$	3.643		h	0.700		h_i	0.973	0.570
	$t_{1/2,i}$	0.748	26.811	$t_{1/2}$	3.511		$t_{1/2}$	2.936	
				$t_{1/2,i}$	3.364	3.516	$t_{1/2,i}$	0.269	9.065
	R^2	0.990		R^2	0.984		R^2	0.998	
	χ^2	0.242		χ^2	0.127		χ^2	0.067	
300	q	25.698		q	27.835		q	27.763	
	k_i	0.9364	0.0263	k_i'	0.1507	0.1537	k_i'	0.799	0.122
	f_i	0.414	0.586	f_i	0.486	0.514	f_i	0.142	0.858
	$t_{1/2}$	2.437		h	0.710		h_i	0.981	0.643
	$t_{1/2,i}$	0.740	27.726	$t_{1/2}$	2.536		$t_{1/2}$	2.234	
				$t_{1/2,i}$	2.391	2.459	$t_{1/2,i}$	0.238	5.970
	R^2	0.988		R^2	0.980		R^2	0.993	
	χ^2	0.273		χ^2	0.247		χ^2	0.208	
350	q	27.301		q	29.375		q	29.6731	
	k_i	0.9425	0.0287	k_i'	0.1562	0.1554	k_i'	0.807	0.138
	f_i	0.441	0.559	f_i	0.492	0.508	f_i	0.101	0.899
	$t_{1/2}$	1.823		h	0.716		h_i	0.983	0.674
	$t_{1/2,i}$	0.735	24.151	$t_{1/2}$	2.070		$t_{1/2}$	1.897	
				$t_{1/2,i}$	1.583	1.806	$t_{1/2,i}$	0.214	4.551
	R^2	0.977		R^2	0.972		R^2	0.992	
	χ^2	0.620		χ^2	0.501		χ^2	0.441	
400	q	29.214		q	31.477		q	31.65	
	k_i	0.9632	0.0296	k_i'	0.1576	0.1573	k_i'	0.825	0.146
	f_i	0.470	0.530	f_i	0.491	0.509	f_i	0.086	0.914
	$t_{1/2}$	1.346		h	0.720		h_i	0.984	0.693
	$t_{1/2,i}$	0.692	23.417	$t_{1/2}$	1.676		$t_{1/2}$	1.156	
				$t_{1/2,i}$	1.119	1.210	$t_{1/2,i}$	0.116	3.057
	R^2	0.976		R^2	0.974		R^2	0.995	
	χ^2	0.683		χ^2	0.468		χ^2	0.332	

parameters of mexp, f-mexp, and modified f-mexp models are listed in Table 4. Tables S1−S3 show the obtained fitting results of PFO, PSO, MO, f-PFO, f-PSO, and f-MO kinetic models. Outcomes indicate that the increase in the initial concentration of the adsorbate leads to the increment in the kinetic rate coefficients and the fractal exponents. The rise in the fractal behavior with the initial concentration of the solute could be ascribed to the increase in the fractal adsorption. These results are consistent with those reported in the literature for other adsorption kinetic systems.[21−23] Also from Table 4, it can be seen that the fractional fractal exponent is larger for the fast step than that of the slow one. Moreover, the comparison between the fitting parameters (k_i', f_i) of the f-mexp model and that of the modified one indicates that the fast and slow steps were significantly differentiated by introducing the fractional fractal exponent to each stage of

https://dx.doi.org/10.1021/acsomega.9b04088
ACS Omega 2020, 5, 5105−5115

the adsorption process. On the other hand, the kinetic half-times were reduced with an increase in the initial concentration of the adsorbate. In fact, the rise in the initial concentration of the solute results in an increment in the adsorption rate, thereby decreasing in the kinetic half-time. Similar observations were reported by El Boundati et al.[23]

Furthermore, the fractional adsorption half-times, $t_{1/2,i}$, were calculated for mexp, f-mexp, and modified f-mexp equations and are listed in Table 4. The results indicate that the fractional adsorption half-times for the fast steps are much shorter than those of the slow stages (<1 min). It should be emphasized, however, that the calculated $t_{1/2,i}$ values from the f-mexp equation do not show significant differences between the fast and slow stages. This could be ascribed to the fact that the kinetic parameters (k_i' and f_i) were fitted by assuming a global fractal exponent h for the f-mexp equation (see Table 4). Thus, the fast and slow steps were not differentiated.

Also, from Tables 4 and S1−S3, we can conclude that each fractal-like kinetic model gives a better adsorption prediction when compared to its classical formulation as confirmed by the highest R^2 value and the lowest χ^2 value. Figure 4 represents

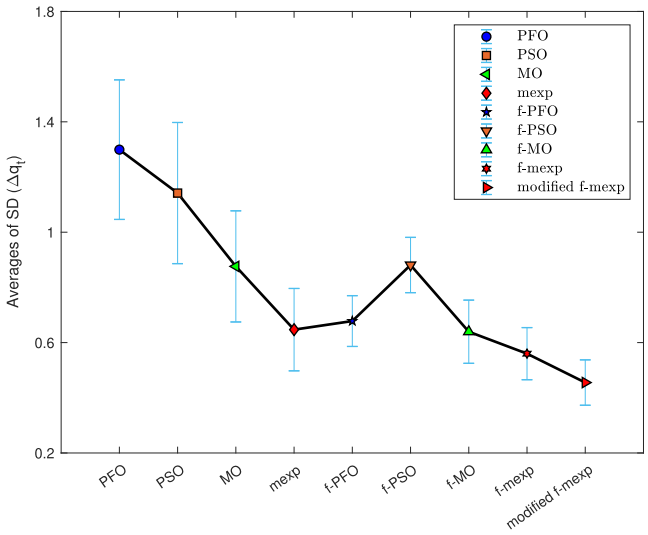

Figure 4. Comparison of average standard deviations (Δq_t) for the tested kinetic models for adsorption of copper onto TATP.

the averages of standard deviations (SDs) of the difference between experimental and calculated adsorbed amounts, Δq_t ($\Delta q_t = q_{t,\mathrm{exp}} - q_{t,\mathrm{cal}}$), from the classical and fractal-like kinetic equations. The results and the plot of Figure 4 show that the modified f-mexp equation is the best one for the analysis of experimental data of copper adsorption on TATP.

The time evolution of the instantaneous adsorption rate coefficient k_{f_i} of the modified f-mexp model, obtained by applying eqs 13 and 16 for the TATP-Cu system, has been plotted in Figure 5. Figure S2 depicts the variation of k_f with the time of the f-mexp, f-MO, f-PSO, and f-PFO models for the adsorption of copper onto TATP. The plots of figures clearly show that k_f is not a constant parameter and it decreases as the time increases. This time dependency means that the history of the process can affect the rate coefficient of adsorption.[19,22] The decrease in the instantaneous rate coefficient with time could also be explained by considering the equilibrium studies. It was found that the TATP surface is heterogeneous; hence, bypassing time, the probability of adsorption on sites with a lower value of the rate constant is increased.[22] Also, it should be noted that the instantaneous rate coefficients of the fast steps (k_{f_1}) decrease faster with time for different initial concentrations of the solute than those of the slow ones (k_{f_2}) because the corresponding fractional fractal exponent values were much higher in comparison with those of the slow stages (see Table 4).

The predictive performance of the modified f-mexp equation has been tested for the modeling of adsorption kinetics of four experimental systems.[50−53] The results are evaluated based on the mathematical error functions R^2 and χ^2. The obtained values of the fitting error functions are listed in Table 5. Figure 6 depicts the results of kinetic modeling by applying the modified f-mexp equation. Outcomes indicate that the modified f-mexp equation can fit the experimental data very well over the whole adsorption range.

4. CONCLUSIONS

The main purpose of this work was to better understand the fractal adsorption kinetics process stages and provide useful information for the interaction mechanism occurring at a solid/solution interface. To this end, we introduced some modifications to the fractal-like multiexponential kinetic equation to take into consideration the fractal behavior for each step of the adsorption process. The applicability of the new equation was verified for the adsorption kinetics of copper onto TATP. The modeling results show a high accuracy

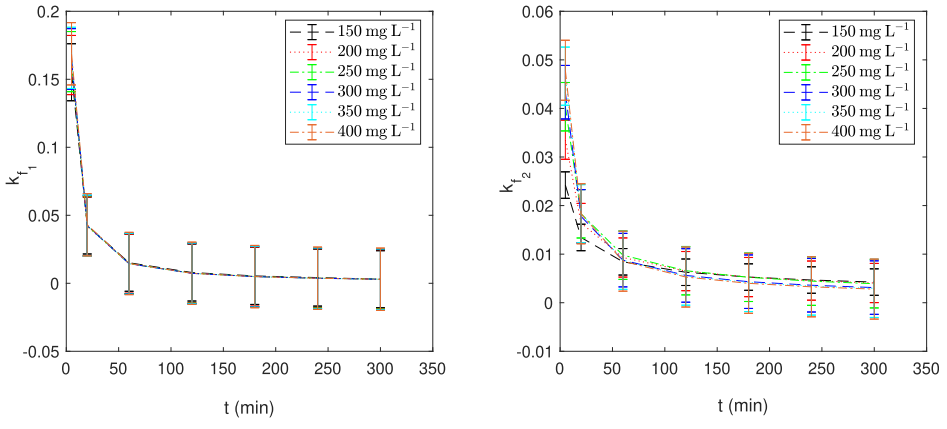

Figure 5. Instantaneous rate coefficient vs time of the modified f-mexp for adsorption of copper onto TATP.

https://dx.doi.org/10.1021/acsomega.9b04088
ACS Omega 2020, 5, 5105−5115

Table 5. Fitting Error Function Values Obtained by Applying the Modified Fractal-Like Multiexponential Equation to the Experimental Data of Adsorption Kinetics from the Literature

	C_i (mg L^{-1})	R^2	χ^2
Boudrahem et al.[50]	10	0.992	0.067
	30	0.998	0.040
	50	0.999	0.015
	70	0.996	0.165
	90	0.999	0.015
Balsamo and Montagnaro[51]	50 (CCA)	0.997	0.035
	50 (F25)	0.998	0.023
	50 (DG10)	0.995	0.026
	50 (SG10)	0.984	0.115
Roy et al.[52]	10	0.989	0.009
	50	0.999	0.002
	100	0.997	0.003
	150	0.991	0.005
	200	0.994	0.002
	250	0.989	0.011
Shi et al.[53]	30	0.998	0.035
	50	0.998	0.048
	70	0.999	0.024
	100	0.996	0.161

between theoretical and experimental data in the whole time range.

The comparison between the fitting results of the new model and those of classical and fractal-like kinetics models indicates that the modified fractal-like multiexponential equation is the best one to describe experimental data of adsorption kinetics for TATP-Cu over the whole adsorption range. The kinetic parameters were affected by the change of adsorbate concentration. Furthermore, the fractal-like adsorption behavior and the kinetic constants were much higher for the fast steps of adsorption in comparison with those of the slow ones.

We also concluded from the modeling analysis of adsorption equilibrium data of copper onto TATP that there is no multisite occupancy effect and that the equilibrium data fit well the Langmuir–Freundlich isotherm, thus reflecting an energetically heterogeneous surface for the TATP.

Moreover, the influence of various parameters such as the adsorbent dose, the solution pH, and the initial solute concentration was studied based on the process simulation by ANNs. The results indicated that the MLP network can better simulate equilibrium data under various experimental conditions with respect to the SLFN.

5. EXPERIMENTAL SECTION

5.1. Adsorbent and Adsorbate. The attapulgite (ATP) samples were obtained from the north of Morocco. The samples were ground by mortar and treated with hydrochloric acid (analytical reagent grade, Sigma-Aldrich) 37% at a concentration of 3 mol L^{-1} for 12 h. The TATP was thoroughly washed with bidistilled water to remove all acid and filtered. The resulting material was termed TATP and used in the adsorption experiments. TATP was dried in the oven at 373 K for 12 h and then sieved to obtain particles smaller than

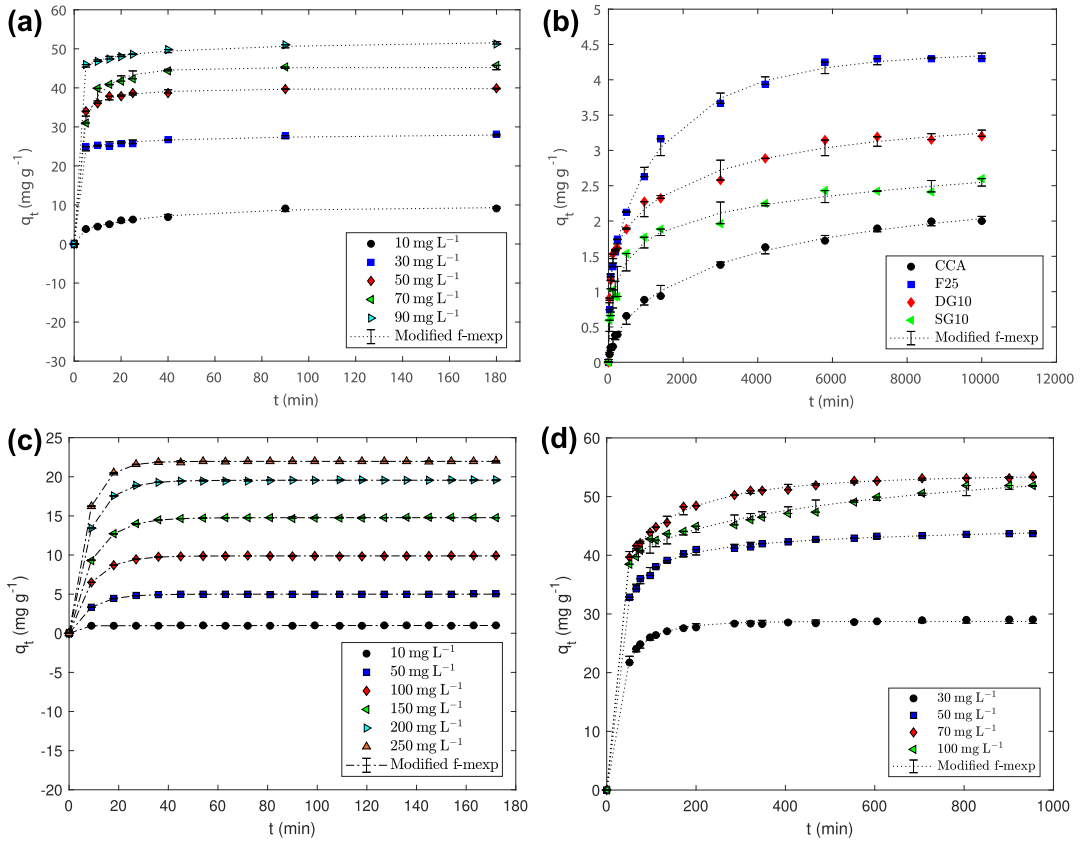

Figure 6. Variation of q_t with time based on the modified f-mexp equation for tested systems (a–d). Lines are the calculated values, and the symbols are the experimental values.

https://dx.doi.org/10.1021/acsomega.9b04088
ACS Omega 2020, 5, 5105–5115

63 μm. This particle size range was selected based on the results of the particle size effect on copper adsorption onto TATP (Figure S3). The aqueous solutions of the adsorbate were prepared by dissolving the desired amount of copper salt ($CuSO_4{\cdot}5H_2O$) (analytical reagent grade, Riedel-de Haën) in redistilled water.

5.2. Potentiometric Titration and Adsorption Experiments. Potentiometric titration was used to evaluate the acid−base nature of the surface properties of ATP and TATP. The ATP or TATP sample (0.5 g) was mixed with 50 mL of NaCl (Carlo Erba Reagents) at various ionic strengths (I = 0.01−0.1 mol L^{-1}). The mixture was acidified by 0.1 M of HCl and then titrated by 0.1 M of NaOH (analytical reagent grade, Fluka). Based on the titration curves pH = $f(V_{NaOH})$, the quantity of the surface charge Q_H (mol g^{-1}) and the PZC were determined.

Adsorption equilibrium experiments were carried out at room temperature by using a batch technique. An amount of TATP was mixed with 25 mL of 150, 200, 250, 300, 350, and 400 mg L^{-1} of copper solutions. The mixture was agitated for 4 h to assure the adsorption equilibrium. The contact time was chosen based on preliminary kinetic tests as largely sufficient to achieve equilibrium conditions (Figure S4). The centrifugation technique was used to separate the solid, and the residual copper concentration was analyzed through atomic absorption spectrophotometry using a spectrophotometer (Jobin Yvon 2). The adsorbent dose effect was conducted by varying the TATP amount from 2 to 12 mg L^{-1}. The effect of pH on the copper adsorption process was investigated in the pH range of 1−5 by adding an appropriate amount of HCl (0.1 M) or NaOH (0.1 M) solutions. The adsorption kinetic experiments were conducted, as in the equilibrium studies, by contacting 8 g L^{-1} of TATP with 25 mL of adsorbate at concentrations ranging from 150 to 400 mg L^{-1}, at time intervals varying from 5 to 300 min.

The adsorption capacity of the adsorbent is obtained by the following equation[23]

$$q_t = \frac{C_i - C_t}{d} \tag{19}$$

where q_t (mg g^{-1}) is the adsorbed amount at the time t, C_i and C_t (mg L^{-1}) are the solute concentrations in the bulk solution initially and at the time t, respectively, and d (g L^{-1}) is the adsorbent dose.

The kinetic half-time, $t_{1/2}$, is the time necessary to adsorb half of the equilibrium quantity (q).[54] It is computed by fixing the adsorption fraction, q_t/q, to one-half.

■ ASSOCIATED CONTENT

Supporting Information

The Supporting Information is available free of charge at https://pubs.acs.org/doi/10.1021/acsomega.9b04088.

MATLAB code for the modified multiexponential equation, extreme learning machine algorithm and the multilayer perceptron neural network, X-ray diffractograms of raw material (ATP) and TATP, fitting parameters of PFO, PSO, mixed 1,2-order models, and their fractal counterparts for copper adsorption onto ATP at different initial concentrations of the solute, variation of k_f with time for the fractal-like mexp, MO, PSO, and PFO models, results of the effect of particle size on copper adsorption onto treated ATP (TATP), contact time effect on copper sorption at different initial concentrations of the solute (PDF)

■ AUTHOR INFORMATION

Corresponding Author

Khadija Ziat − *Laboratoire Physico-Chimie des Matériaux, Substances Naturelles et Environnement, Faculty of Sciences and Techniques, Abdelmalek Essaâdi University, Tangier 90040, Morocco*; orcid.org/0000-0003-0256-5083; Email: khadijaziat@gmail.com

Authors

Naoual El Bardiji − *Laboratoire Physico-Chimie des Matériaux, Substances Naturelles et Environnement, Faculty of Sciences and Techniques, Abdelmalek Essaâdi University, Tangier 90040, Morocco*

Ahmed Naji − *Laboratoire de Mathématiques et Applications, Faculty of Sciences and Techniques, Abdelmalek Essaâdi University, Tangier 90040, Morocco*

Mohamed Saidi − *Laboratoire Physico-Chimie des Matériaux, Substances Naturelles et Environnement, Faculty of Sciences and Techniques, Abdelmalek Essaâdi University, Tangier 90040, Morocco*

Complete contact information is available at: https://pubs.acs.org/10.1021/acsomega.9b04088

Notes

The authors declare no competing financial interest.

■ NOMENCLATURE

β_i	weight vector connecting of the output neuron
χ^2	chi-squared error
N	number of hidden neurons
$[H^+]$	concentration of H^+ (mol L^{-1})
$[OH^-]$	concentration of OH^- (mol L^{-1})
σ	spread parameter for RBF
θ	coverage
a	weight vector of the hidden neuron
a_{LF}	Langmuir−Freundlich constant
b	threshold of the ith hidden neuron
C	solute concentration in the bulk solution at equilibrium (mg L^{-1})
c	center of RBF
C_a	concentration of the acid (mol L^{-1})
C_b	concentration of the base (mol L^{-1})
C_i	initial solute concentration in the bulk solution (mg L^{-1})
C_t	solute concentration in the bulk solution at the time t (mg L^{-1})
D	number of input neurons
d	adsorbent dose (g L^{-1})
f	activation function
h	fractal exponent
h_i	fractional fractal exponent
k'	time-independent rate coefficient
k'_1	kinetic constant for the fractal-like pseudo-first-order model ($min^{-(1-h)}$)
k'_2	kinetic constant for the fractal-like pseudo-second-order model (g $mg^{-1}{\cdot}min^{-(1-h)}$)
k'_i	kinetic constant for the fractal-like multiexponential model ($min^{-(1-h)}$)
k_1	rate constant of PFO adsorption (min^{-1})

https://dx.doi.org/10.1021/acsomega.9b04088
ACS Omega 2020, 5, 5105−5115

k_2	rate constant of PSO adsorption (g mg^{-1} min^{-1})
K_e	equilibrium constant
K_F	Freundlich constant
k_f	fractal instantaneous rate coefficient
k_i	rate constant of multiexponential model (min^{-1})
K_{LF}	Langmuir−Freundlich constant
q	adsorbed amount at equilibrium (mg g^{-1})
Q_H	quantity of surface charge (mol g^{-1})
q_t	adsorbed amount at the time t (mg g^{-1})
q_{max}	theoretical monolayer capacity (mg g^{-1})
R^2	coefficient of determination
s	heterogeneity constant
t	time (min)
$t_{1/2}$	kinetic half-time (min)
x	input vector
ANN	artificial neural network
ATP	attapulgite
ELM	extreme learning machine
k	number of sites
MLP	multilayer perceptron
N	number of experimental data
n	number of exponential terms
p	equilibrium pressure (Pa)
PZC	point of zero charge
RBF	radial basis function
SLFN	single-layer feedforward neural network
TATP	treated ATP
V	volume (L)

SUBSCRIPTS

cal	calculated
exp	experimental

REFERENCES

(1) Uddin, M. K. A review on the adsorption of heavy metals by clay minerals, with special focus on the past decade. *Chem. Eng. J.* **2017**, *308*, 438−462.

(2) Balsamo, M.; Montagnaro, F. Liquid−solid adsorption processes interpreted by fractal-like kinetic models. *Environ. Chem. Lett.* **2019**, *17*, 1067−1075.

(3) Sarve, A.; Sonawane, S. S.; Varma, M. N. Ultrasound assisted biodiesel production from sesame (Sesamum indicum L.) oil using barium hydroxide as a heterogeneous catalyst: Comparative assessment of prediction abilities between response surface methodology (RSM) and artificial neural network (ANN). *Ultrason. Sonochem.* **2015**, *26*, 218−228.

(4) Ali, I.; Alharbi, O. M. L.; Alothman, Z. A.; Badjah, A. Y.; Alwarthan, A.; Basheer, A. A. Artificial neural network modelling of amido black dye sorption on iron composite nano material: Kinetics and thermodynamics studies. *J. Mol. Liq.* **2018**, *250*, 1−8.

(5) Tanzifi, M.; Yaraki, M. T.; Kiadehi, A. D.; Hosseini, S. H.; Olazar, M.; Bharti, A. K.; Agarwal, S.; Gupta, V. K.; Kazemi, A. Adsorption of amido black 10B from aqueous solution using polyaniline/SiO_2 nanocomposite: Experimental investigation and artificial neural network modeling. *J. Colloid Interface Sci.* **2018**, *510*, 246−261.

(6) Sharafi, K.; Pirsaheb, M.; Gupta, V. K.; Agarwal, S.; Moradi, M.; Vasseghian, Y.; Dragoi, E.-N. Phenol adsorption on scoria stone as adsorbent—Application of response surface method and artificial neural networks. *J. Mol. Liq.* **2019**, *274*, 699−714.

(7) Foo, K. Y.; Hameed, B. H. Insights into the modeling of adsorption isotherm systems. *Chem. Eng. J.* **2010**, *156*, 2−10.

(8) Langmuir, I. The constitution and fundamental properties of solids and liquids. Part I. Solids. *J. Am. Chem. Soc.* **1916**, *38*, 2221−2295.

(9) Freundlich, H. Über die adsorption in lösungen. *Z. Phys. Chem.* **1907**, *57U*, 385−470.

(10) Nitta, T.; Shigetomi, T.; Kuro-Oka, M.; Katayama, T. An adsorption isotherm of multi-site occupancy model for homogeneous surface. *J. Chem. Eng. Jpn.* **1984**, *17*, 39−45.

(11) Nitta, T.; Kuro-Oka, M.; Katayama, T. An adsorption isotherm of multi-site occupancy model for heterogeneous surface. *J. Chem. Eng. Jpn.* **1984**, *17*, 45−52.

(12) Ramirez-Pastor, A. J.; Eggarter, T. P.; Pereyra, V. D.; Riccardo, J. L. Statistical thermodynamics and transport of linear adsorbates. *Phys. Rev. B: Condens. Matter Mater. Phys.* **1999**, *59*, 11027.

(13) Ramirez-Pastor, A. J.; Pereyra, V. D.; Riccardo, J. L. Statistical thermodynamics of linear adsorbates in low dimensions: Application to adsorption on heterogeneous surfaces. *Langmuir* **1999**, *15*, 5707−5712.

(14) Riccardo, J. L.; Ramirez-Pastor, A. J.; Romá, F. Multilayer adsorption with multisite occupancy: An improved isotherm for surface characterization. *Langmuir* **2002**, *18*, 2130−2134.

(15) Romá, F.; Ramirez-Pastor, A. J.; Riccardo, J. L. Multisite occupancy adsorption: Comparative study of new different analytical approaches. *Langmuir* **2003**, *19*, 6770−6777.

(16) Riccardo, J. L.; Ramirez-Pastor, A.; Romá, F. Fractional statistical theory of adsorption of polyatomics. *Phys. Rev. Lett.* **2004**, *93*, 186101.

(17) Riccardo, J. J.; Riccardo, J. L.; Ramirez-Pastor, A. J.; Pasinetti, P. M. Multiple Exclusion Statistics. *Phys. Rev. Lett.* **2019**, *123*, 020602.

(18) Gupta, S. S.; Bhattacharyya, K. G. Kinetics of adsorption of metal ions on inorganic materials: A review. *Adv. Colloid Interface Sci.* **2011**, *162*, 39−58.

(19) Kopelman, R. Fractal reaction kinetics. *Science* **1988**, *241*, 1620−1626.

(20) Brouers, F.; Sotolongo-Costa, O. Generalized fractal kinetics in complex systems (application to biophysics and biotechnology). *Phys. Stat. Mech. Appl.* **2006**, *368*, 165−175.

(21) Haerifar, M.; Azizian, S. Fractal-like adsorption kinetics at the solid/solution interface. *J. Phys. Chem. C* **2012**, *116*, 13111−13119.

(22) Haerifar, M.; Azizian, S. Fractal-like kinetics for adsorption on heterogeneous solid surfaces. *J. Phys. Chem. C* **2014**, *118*, 1129−1134.

(23) El Boundati, Y.; Ziat, K.; Naji, A.; Saidi, M. Generalized fractal-like adsorption kinetic models: Application to adsorption of copper on Argan nut shell. *J. Mol. Liq.* **2019**, *276*, 15−26.

(24) Bebana, M. V.; Ziat, K.; Semlal, N.; Saidi, M. Modeling compressive strength of Moroccan fly ash−phosphogypsum geopolymer bricks. *SN Appl. Sci.* **2019**, *1*, 1666.

(25) Huang, G.-B.; Zhu, Q.-Y.; Siew, C.-K. Extreme learning machine: Theory and applications. *Neurocomputing* **2006**, *70*, 489−501.

(26) Huang, G.-B.; Chen, L.; Siew, C.-K. Universal approximation using incremental constructive feedforward networks with random hidden nodes. *IEEE Trans. Neural Network.* **2006**, *17*, 879−892.

(27) Huang, G.; Huang, G.-B.; Song, S.; You, K. Trends in extreme learning machines: A review. *Neural Network.* **2015**, *61*, 32−48.

(28) Harpham, C.; Dawson, C. W. The effect of different basis functions on a radial basis function network for time series prediction: A comparative study. *Neurocomputing* **2006**, *69*, 2161−2170.

(29) Hornik, K.; Stinchcombe, M.; White, H. Multilayer feedforward networks are universal approximators. *Neural Network.* **1989**, *2*, 359−366.

(30) Gardner, M. W.; Dorling, S. R. Artificial neural networks (the multilayer perceptron) a review of applications in the atmospheric sciences. *Atmos. Environ.* **1998**, *32*, 2627−2636.

(31) Haykin, S. S. *Neural Networks and Learning Machines*; Pearson Education: Upper Saddle River, 2009.

(32) Patra, T. K.; Meenakshisundaram, V.; Hung, J.-H.; Simmons, D. S. Neural-network-biased genetic algorithms for materials design: Evolutionary algorithms that learn. *ACS Comb. Sci.* **2017**, *19*, 96−107.

(33) Song, X.; Qiao, C.; Tao, J.; Bao, B.; Han, X.; Zhao, S. Interfacial engineering of thermoresponsive microgel capsules: Polymeric wetting vs colloidal adhesion. *Macromolecules* **2019**, *52*, 3869.

https://dx.doi.org/10.1021/acsomega.9b04088
ACS Omega 2020, 5, 5105−5115

(34) Nebaghe, K. C.; El Boundati, Y.; Ziat, K.; Naji, A.; Rghioui, L.; Saidi, M. Comparison of linear and non-linear method for determination of optimum equilibrium isotherm for adsorption of copper(II) onto treated Martil sand. *Fluid Phase Equilib.* **2016**, *430*, 188−194.
(35) Cheung, C. W.; Porter, J. F.; McKay, G. Sorption kinetics for the removal of copper and zinc from effluents using bone char. *Sep. Purif. Technol.* **2000**, *19*, 55−64.
(36) Derylo-Marczewska, A.; Blachnio, M.; Marczewski, A. W.; Swiatkowski, A.; Buczek, B. Adsorption of chlorophenoxy pesticides on activated carbon with gradually removed external particle layers. *Chem. Eng. J.* **2017**, *308*, 408−418.
(37) Lagergren, S. About the theory of so-called adsorption of soluble substances. *K.—Sven. Vetenskapsakademiens Handl.* **1898**, *24*, 1−39.
(38) Ho, Y.; McKay, G. The kinetics of sorption of divalent metal ions onto sphagnum moss peat. *Water Res.* **2000**, *34*, 735−742.
(39) Marczewski, A. W. Kinetics and equilibrium of adsorption of organic solutes on mesoporous carbons. *Appl. Surf. Sci.* **2007**, *253*, 5818−5826.
(40) Marczewski, A. W. Application of mixed order rate equations to adsorption of methylene blue on mesoporous carbons. *Appl. Surf. Sci.* **2010**, *256*, 5145−5152.
(41) Wang, Z.-W.; Xu, F.; Manchala, K. R.; Sun, Y.; Li, Y. Fractal-like kinetics of the solid-state anaerobic digestion. *Waste Manag.* **2016**, *53*, 55−61.
(42) Hu, Q.; Liu, Y.; Feng, C.; Zhang, Z.; Lei, Z.; Shimizu, K. Predicting equilibrium time by adsorption kinetic equations and modifying Langmuir isotherm by fractal-like approach. *J. Mol. Liq.* **2018**, *268*, 728−733.
(43) Somasundaran, P.; Agar, G. E. The zero point of charge of calcite. *J. Colloid Interface Sci.* **1967**, *24*, 433−440.
(44) Frini-Srasra, N.; Srasra, E. Determination of acid-base properties of HCl acid activated palygorskite by potentiometric titration. *Surf. Eng. Appl. Electrochem.* **2008**, *44*, 401−409.
(45) Xie, X.; Deng, R.; Pang, Y.; Bai, Y.; Zheng, W.; Zhou, Y. Adsorption of copper(II) by sulfur microparticles. *Chem. Eng. J.* **2017**, *314*, 434−442.
(46) Nebagha, K. C.; Ziat, K.; Rghioui, L.; Khayet, M.; Saidi, M.; Aboumaria, K.; EL Hourch, A.; Sebti, S. Adsorptive removal of copper(II) from aqueous solutions using low cost Moroccan adsorbent. Part I: Parameters influencing Cu(II) adsorption. *J. Mater. Environ. Sci.* **2015**, *6*, 3022−3033.
(47) Pellera, F.-M.; Giannis, A.; Kalderis, D.; Anastasiadou, K.; Stegmann, R.; Wang, J.-Y.; Gidarakos, E. Adsorption of Cu(II) ions from aqueous solutions on biochars prepared from agricultural by-products. *J. Environ. Manag.* **2012**, *96*, 35−42.
(48) Taimur, S.; Hassan, M. I.; Yasin, T. Removal of copper using novel amidoxime based chelating nanohybrid adsorbent. *Eur. Polym. J.* **2017**, *95*, 93−104.
(49) Romá, F.; Riccardo, J. L.; Ramirez-Pastor, A. J. Statistical thermodynamics models for polyatomic adsorbates: Application to adsorption of n-paraffins in 5A zeolite. *Langmuir* **2005**, *21*, 2454−2459.
(50) Boudrahem, F.; Aissani-Benissad, F.; Soualah, A. Adsorption of lead(II) from aqueous solution by using leaves of date trees as an adsorbent. *J. Chem. Eng. Data* **2011**, *56*, 1804−1812.
(51) Balsamo, M.; Montagnaro, F. Fractal-like Vermeulen kinetic equation for the description of diffusion-controlled adsorption dynamics. *J. Phys. Chem. C* **2015**, *119*, 8781−8785.
(52) Roy, A.; Adhikari, B.; Majumder, S. B. Equilibrium, kinetic, and thermodynamic studies of azo dye adsorption from aqueous solution by chemically modified lignocellulosic jute fiber. *Ind. Eng. Chem. Res.* **2013**, *52*, 6502−6512.
(53) Shi, H.; Li, W.; Zhong, L.; Xu, C. Methylene blue adsorption from aqueous solution by magnetic cellulose/graphene oxide composite: Equilibrium, kinetics, and thermodynamics. *Ind. Eng. Chem. Res.* **2014**, *53*, 1108−1118.
(54) Gaspard, S.; Altenor, S.; Passe-Coutrin, N.; Ouensanga, A.; Brouers, F. Parameters from a new kinetic equation to evaluate activated carbons efficiency for water treatment. *Water Res.* **2006**, *40*, 3467−3477.

https://dx.doi.org/10.1021/acsomega.9b04088
ACS Omega 2020, 5, 5105−5115